

# Multiple Exciton Generation and Recombination Dynamics in Small Si and CdSe Quantum Dots: An *Ab Initio* Time-Domain Study

Kim Hyeon-Deuk<sup>†,\*</sup> and Oleg V. Prezhdo<sup>‡,\*</sup>

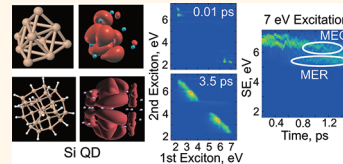
<sup>†</sup>Department of Chemistry, Kyoto University, Kyoto 606-8502, Japan and <sup>‡</sup>Department of Chemistry, University of Rochester, Rochester, New York 14642, United States

The solar spectrum extends over a broad range of energies, and in most photovoltaic materials, high-energy excitations rapidly relax to the lowest excited state at the red end of the spectrum by interaction with phonons.<sup>1</sup> Thus, significant amounts of solar power are lost to heat, limiting the maximum thermodynamic efficiency of a standard photovoltaic device to 32%.<sup>2</sup> Recent time-resolved experiments showed ultrafast electron–phonon relaxation even in nanoscale crystals, similar to that observed in bulk.<sup>3–8</sup> The general expectation that quantum confinement would limit energy losses due to an increased mismatch between the electronic energy gaps and phonon frequencies held at low energies and in perfectly designed quantum dots (QDs).<sup>9</sup> The experimental work has advanced considerably over the past decade,<sup>8</sup> and sophisticated theoretical studies have shown that the photoinduced dynamics in semiconductor QDs involve a complex interplay of many processes.<sup>10</sup>

High-energy electrons can be efficiently extracted from QDs before cooling, provided that they are strongly coupled to a semiconductor substrate, such as TiO<sub>2</sub><sup>11,12</sup> or ITO.<sup>13</sup> As an alternative to hot electron extraction, multiple exciton generation (MEG) provides another route to increased solar cell efficiencies.<sup>14–17</sup> One of the most remarkable features of semiconductor QDs<sup>18–36</sup> and other nanoscale materials<sup>37–41</sup> is that MEG allows creation of multiple charge carriers upon absorption of a single quantum of light. Multiple electron–hole pairs are produced when a highly excited charge carrier relaxes to the band edge while exciting another electron across the band gap. Semiconductor QDs promise higher photovoltaic efficiencies because quantum confinement

**ABSTRACT** Multiple exciton generation and recombination (MEG and MER) dynamics in semiconductor quantum dots (QDs) are simulated using *ab initio* time-dependent density functional theory in combination with nonadiabatic molecular dynamics. The approach differs from other MEG and MER theories because it provides atomistic description, employs time-domain representation, allows for various dynamical regimes, and includes electron–phonon interactions. MEG rapidly accelerates with energy, reflecting strong energy dependence of double exciton (DE) density of states. At early times, MEG is Gaussian rather than exponential. Exponential dynamics, assumed in rate theories, starts at a later time and becomes more important in larger QDs.

Phonon-assisted MEG is observed at energies below the purely electronic threshold, particularly in the presence of high-frequency ligand vibrations. Coupling to phonons is essential for MER since higher-energy DEs must relax to recombine into single excitons (SEs), and SEs formed during MERs must lose some of their energy to avoid recreating DEs. MER simulated starting from a DE is significantly slower than MER involving an optical excitation of a SE, followed by MEG and then MER. The latter time scale agrees with experiment, emphasizing the importance of quantum-mechanical superpositions of many DEs for efficient MER. The detailed description of the interplay between MEG and MER coupled to phonons provides important insights into the excited state dynamics of semiconductor QDs and nanoscale materials in general.



**KEYWORDS:** multiple exciton generation · multiple exciton recombination · Auger/inverse Auger processes · quantum dots · electron–phonon coupling · solar energy conversion

can lead to efficient MEG. MEG yields are higher in QDs than in bulk<sup>14,16,42</sup> because the momentum conservation requirement is lifted in QDs, and the Coulomb interaction between electrons and holes is enhanced due to closer proximity of the charge carriers. Multiple exciton recombination (MER) is the inverse of MEG.<sup>24,35,43–48</sup> In combination with electron–phonon relaxation, it accelerates energy losses to heat by annihilating MEs to SEs of higher energy that is dissipated by phonons. The MEG and MER processes

\* Address correspondence to kim@kuchem.kyoto-u.ac.jp, oleg.prezhdo@rochester.edu.

Received for review October 9, 2011 and accepted January 3, 2012.

Published online January 03, 2012  
10.1021/nn2038884

© 2012 American Chemical Society

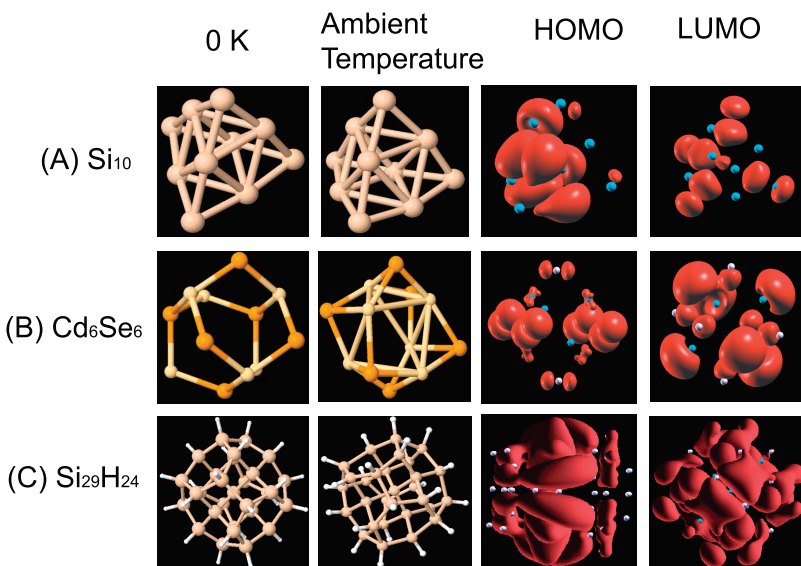


**Figure 1.** QDs used in our simulations, (A)  $\text{Si}_{10}$ , (B)  $\text{Cd}_6\text{Se}_6$ , and (C)  $\text{Si}_{29}\text{H}_{24}$ . Shown from left to right are structures optimized at 0 K, typical structures from a dynamics trajectory at the ambient temperature, and charge densities of the HOMO and LUMO states.

govern exciton dynamics in semiconductor QDs. Understanding and controlling MEG and MER is essential for utilization of the excess photon energy and reduction of energy losses to heat. Presently, conflicting reports have been published on MEG efficiencies, and the dynamics and mechanisms of MEG and MER are still poorly understood and remain controversial.<sup>42,49–55</sup>

Many theoretical studies provide systematic analysis of MEG and MER as a function of QD size, energy, and semiconductor type.<sup>20,22–25,28,30–32,35</sup> Such systematic investigations become largely possible by employing theoretical models that use phenomenological descriptions of QD electronic structure, apply in the perturbative weak-coupling limit, assume exponential decay, exclude phonon dynamics, and describe MEG and MER independently. A complete picture should include simultaneously MEG and MER dynamics, phonon-assisted MEG and MER, and electron–phonon relaxation. Various dynamical regimes should be allowed. Additionally, an atomistic description is needed to study the role of ligands, dopants, unsaturated chemical bonds, and other realistic aspects of QDs, which are not perfect geometric and chemical objects, and often contain many defects. Recently, we developed such time-domain atomistic description.<sup>24</sup> Our method combines *ab initio* time-dependent density functional theory (TDDFT) with nonadiabatic molecular dynamics (NAMD). The simulation gives a novel and comprehensive perspective on the scattering dynamics of excited charge carriers in nanoscale materials and provides important insights into the mechanisms of solar energy harvesting.

## RESULTS AND DISCUSSION

The study focuses on Si and CdSe QDs (Figure 1). CdSe is one of the most popular and well-studied

semiconductor QD materials.<sup>4,5,20,27,31,51</sup> Si QDs deserve particular attention since much of the present photovoltaic industry is already based in Si. Further, Si does not raise toxicity issues that can become a major concern with other materials. Recently, Si QDs demonstrated the potential to make solar devices with higher efficiencies within the developed technologies.<sup>18</sup> In order for Si QDs to become a viable option in solar devices, a theoretical understanding of MEG and MER in Si QDs is necessary. The current work investigates the MEG and MER dynamics in Si QDs of different size and surface passivation and compares the Si results with those for CdSe.

**Geometric and Electronic Structure of QDs.** Figure 1 shows the QDs used in the current study. The clusters are composed of “magic” numbers of atoms<sup>56,57</sup> and are roughly spherical. The smaller QDs,  $\text{Si}_{10}$  and  $\text{Cd}_6\text{Se}_6$ , are close in size and contain similar numbers of atoms. Their surfaces remain bare. As a result, the atoms of  $\text{Si}_{10}$  and  $\text{Cd}_6\text{Se}_6$  are missing some of the bonds that would be present in the corresponding bulk materials. These “dangling” bonds are “healed” by cluster reconstruction, which does preserve the topology of the corresponding bulk structure. Dangling bond healing creates a substantial energy gap,  $E_g$ , between the lowest unoccupied molecular orbital (LUMO) and the highest occupied molecular orbital (HOMO). However, the gaps are not as large as one may predict using, for instance, the effective mass theory.<sup>21</sup> The larger cluster,  $\text{Si}_{29}\text{H}_{24}$ , contains an additional layer of Si atoms relative to  $\text{Si}_{10}$ . The surface of the larger cluster is passivated by hydrogens, representing QD ligands that are present in QDs obtained by solution chemistry. The ligands do a better job eliminating dangling bonds than surface reconstruction alone. As a result, the HOMO–LUMO

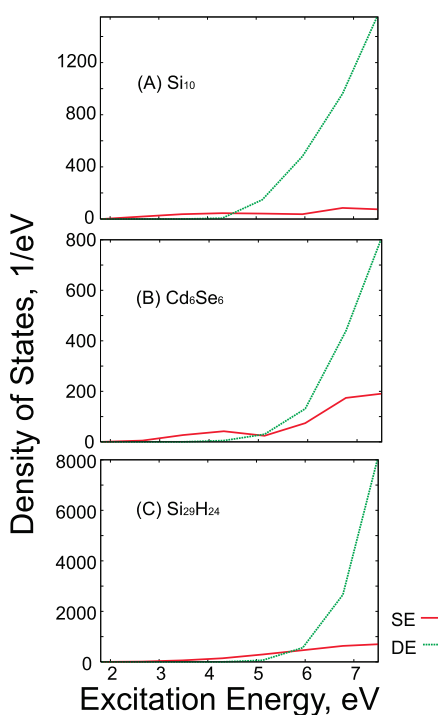


**Figure 2.** SE and DE DOS of (A)  $\text{Si}_{10}$ , (B)  $\text{Cd}_6\text{Se}_6$ , and (C)  $\text{Si}_{29}\text{H}_{24}$ . The lowest-energy SEs are at (A) 2.0 eV, (B) 2.0 eV, and (C) 2.1 eV. The DE DOS starts at higher energies than the SE DOS. The former exceeds the latter at 2.5–2.8 times the lowest SE energy. The DOS is much higher in  $\text{Si}_{29}\text{H}_{24}$  than in the smaller QDs, and the DE/SE DOS ratio increases most rapidly.

energy gap of the larger Si cluster is very close to that for the smaller Si and CdSe clusters, even though a particle-in-a-sphere type description predicts the gap to be inversely proportional to the QD diameter.<sup>36,46–48</sup> This particular choice of the systems allows us to study the MEG and MER processes within the same energy range for the three clusters of different size and material and emphasizes the importance of the atomistic aspects of QD structure and the role of the ligands.

The left column of Figure 1 shows the QDs fully optimized at 0 K. The structures in the midleft column are snapshots from the dynamics simulation at ambient temperature. Thermal fluctuations of atoms induce significant distortions in the QD geometry. The two smaller clusters change their shapes more notably than the largest QD, and  $\text{Cd}_6\text{Se}_6$  experiences a larger reconstruction than  $\text{Si}_{10}$ . However, all QDs preserve the bulk topology at room temperature: the bond lengths fluctuate significantly, but the bonds do not break, and the key elements of the QD electronic structure remain intact. For instance, the HOMO–LUMO energy gap fluctuates only within a few percent during the trajectory, and no defect states appear within the gap.

The panels in the midright and right columns of Figure 1 display the HOMO and LUMO charge densities. The orbitals appear notably more localized on the atoms in the smaller clusters, compared to the  $\text{Si}_{29}\text{H}_{29}$  QD, where the HOMO and LUMO are delocalized

over the whole core region. The bonding pattern is more homogeneous in the larger system, allowing for a uniform spread of the hole and electron densities. The hydrogen ligands passivating the  $\text{Si}_{29}\text{H}_{29}$  surface contribute somewhat to the orbital densities, with the LUMO delocalized onto the hydrogens more substantially than the HOMO. Note the smaller number of white spheres seen in the LUMO picture relative to the HOMO.

The single exciton (SE) and double exciton (DE) density of states (DOS) of the three QDs are shown in Figure 2. The underlying atomic structure, thermal fluctuations, and Coulomb interactions break electronic state degeneracies that appear in a particle-in-a-sphere type model. A complicated multilevel band structure is therefore created, resulting in continuous DOS even in the very small QDs. The lowest-energy SEs appear at similar energies in the three clusters: 2.0, 2.0, and 2.1 eV for  $\text{Si}_{10}$ ,  $\text{Cd}_6\text{Se}_6$ , and  $\text{Si}_{29}\text{H}_{24}$ , respectively. The DOS is notably larger in  $\text{Si}_{29}\text{H}_{24}$  than in the smaller QDs; compare the y-scales of the different panels in Figure 2. The DE DOS starts at a higher energy than the SE DOS. At the same time, it rises much more steeply. Because the combinatorial number of DEs grows significantly faster with energy than the number of SEs, the DE DOS completely dominates over the SE DOS at higher energies. The threshold energy at which the DE DOS becomes greater than the SE DOS occurs at about  $2.4\text{--}2.8E_g$ . The threshold is slightly lower in the smaller clusters, where the SE DOS exhibits dips in the relevant energy region. The difference between the DOS of the small and large QDs is greater for DEs than for SEs. At high energies, the ratio of the DE DOS to the SE DOS is largest for  $\text{Si}_{29}\text{H}_{24}$ . The analysis of the SE and DE DOS immediately suggests that the excited state population will shift to DEs at high energies and to SEs at low energies, provided that SEs and DEs are coupled.

**Multiple Exciton Generation.** Figure 3 describes the MEG dynamics starting from an initially excited SE state, which has the displayed energy. The initial state couples to other SE and DE states. The decay of the total population of all SEs, shown in Figure 3, is a result of MEG. Our simulation includes SEs, DEs, and the ground state. The ground state population remains negligible throughout the simulation, in agreement with experiments,<sup>58–61</sup> which show that the nonradiative relaxation to the ground electronic state takes place on a nanosecond time scale. The nonradiative relaxation to the ground electronic state quenches fluorescence in semiconductor QDs.

The MEG dynamics is strongly influenced by the energy of the initial excitation. The energy dependence of the MEG rate arises mainly from the rapid growth of the DE DOS with energy (Figure 2). As a result, more highly excited SEs are able to couple to a significantly larger number of DEs. The MEG dynamics is faster in  $\text{Si}_{10}$  than in  $\text{Cd}_6\text{Se}_6$ , as indicated by lines

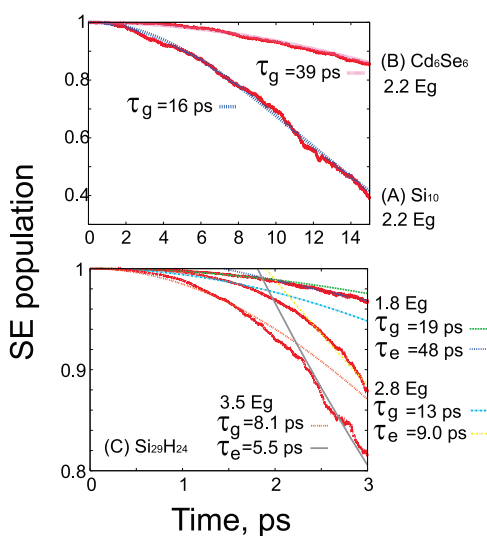


**Figure 3.** Decay of the total population of all SEs starting from the initially excited SE with the displayed energy. The decay is due to MEG. The decay is Gaussian in the two smaller dots; it is faster in  $\text{Si}_{10}$  than in  $\text{Cd}_6\text{Se}_6$ . The MEG dynamics in  $\text{Si}_{29}\text{H}_{24}$  exhibits a transition from the Gaussian to the exponential regime. Slow phonon-assisted MEG is observed at energies below  $2E_g$  in  $\text{Si}_{29}\text{H}_{24}$ , which possesses high-frequency hydrogen phonons. The Gaussian and exponential time scales,  $\tau_g$  and  $\tau_e$ , are displayed.

A and B in the upper panel of Figure 3. This is because the ratio of the DE DOS over the SE DOS is larger in  $\text{Si}_{10}$  than in  $\text{Cd}_6\text{Se}_6$ . As shown for  $\text{Si}_{29}\text{H}_{24}$  in the lower panel of Figure 3, the MEG rate increases significantly with energy. SE states of higher energies are in resonance with a much higher density of DE states. The strong energy dependence of the MEG rate seen in our calculations is in agreement with the earlier theories.<sup>20,22–25,28,30–32,35,37</sup>

The current simulation of the MEG dynamics differs from the earlier studies in two very important aspects. First, our study explicitly includes electron–phonon coupling (see the Simulation Methods section) and, as a result, allows for phonon-assisted Auger processes. In particular, the simulations show phonon-assisted MEG starting at energies lower than  $2E_g$ , as illustrated by the top line in the lower panel of Figure 3. Notably slower than MEG at energies above  $2E_g$ , phonon-assisted MEG becomes possible at energies below  $2E_g$  largely due to the high-frequency Si–H phonons in the  $\text{Si}_{29}\text{H}_{24}$  QD. A single quantum of the Si–H phonon is on the order of 0.25 eV. The electronic degrees of freedom can borrow this amount of energy from phonons and produce MEG below the purely electronic threshold.

The second major difference of the current simulation from the earlier theories resides in the explicit time-domain representation of MEG. Most other theories compute MEG rates,<sup>20,23,28,30–32,34,37,53</sup> thereby assuming that MEG is an exponential process. In general, quantum dynamics starts as a Gaussian process, and only later becomes exponential. The Gaussian component of quantum dynamics is the source of the quantum Zeno effect,<sup>62,63</sup> in which frequent

measurements of the quantum subsystem completely stop its evolution. Such measurements can be performed by an outside observer or, effectively, by the environment, such as the phonon modes of the QD itself, ligands, solvent, etc. The transition from the Gaussian to the exponential regime occurs when the number of quantum states accessible to system's dynamics becomes large. Further, rate expressions, such as Fermi's golden rule, are derived in the weak-coupling perturbative limit, while our calculation is nonperturbative. In the presence of strong electron–hole coupling caused by quantum confinement, perturbative treatments could become invalid, especially in small QDs, in which the confinement effect is strongest.

The MEG dynamics in the smaller QDs can be well fitted by the Gaussian functions (see top panel of Figure 3). This result emphasizes the fact that the density of DE states coupled to the SE states is relatively small in  $\text{Si}_{10}$  and  $\text{Cd}_6\text{Se}_6$ , and that a rate description, such as Fermi's golden rule, is not applicable. The MEG data in the large QD can be fitted by a combination of Gaussian and exponential functions. The transition from the Gaussian to the exponential behavior happens relatively early in the  $\text{Si}_{29}\text{H}_{24}$  QD, after about 2 ps. The amplitude of the Gaussian decay grows with energy. Since only about 10% of the overall decay amplitude is Gaussian, the rate description of MEG implicitly assuming exponential decay should be valid for intermediate and large QDs with high DOS.

Figure 4 shows the evolution of the population of the initially excited SE states. The lifetime of the initially excited SE states is much shorter than the MEG time (Figure 3). This fact demonstrates that, at the early stage, the excited SEs diffuse into other SEs rather than into DEs. Thus, at very short times, the SE evolution is determined mainly by the SE DOS. The initial SEs of  $\text{Si}_{10}$  and  $\text{Cd}_6\text{Se}_6$  have similar lifetimes on the order of 1–3 ps (Figure 3A,B). Note that the MEG times for these QDs are on the order of 15–40 ps (Figure 3). Recurrences and partial repopulation of the initial SE states is seen in the smaller dots at times as long as 10–15 ps. The population of the initial SEs decays within 1 ps in the larger  $\text{Si}_{29}\text{H}_{24}$  QD (Figure 4C). The decay is faster than in the smaller crystals due to higher SE and DE DOS. The lowest-energy SE,  $1.8E_g$ , survives longer than the SEs of higher energy because of the lower SE DOS at this energy (Figure 2).

It should be noted that the simulated inverse Auger process, also known as impact ionization,<sup>23,33</sup> constitutes one of the three proposed MEG mechanisms. The other two are the direct<sup>34</sup> and dephasing<sup>21</sup> mechanisms. The direct process suggests that MEs are generated immediately upon absorption of light. In order to study this mechanism, the QD–light interaction should be considered explicitly. The dephasing mechanism suggests that a coherent superposition between SE

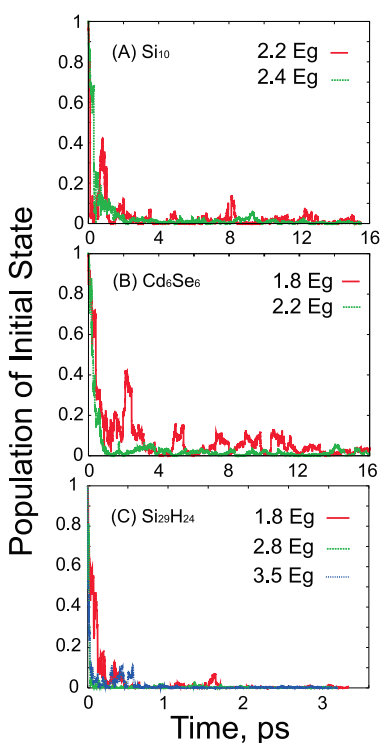


**Figure 4.** Population decay of the initially excited SE states. The decay is faster in larger dots and at higher energies. Note that the initial SE state decay is much faster than the decay of the total population of all SE states (Figure 3). Hence, the initial SE state transfers its population not only to DEs, resulting in MEG, but also to other SEs.

and ME states is created by either light or Coulomb interaction, and that the superposition dephases primarily *via* MEs since MEs couple to phonons more strongly than SEs. Previously, we have studied the two alternative mechanisms independently.<sup>22,25,64,65</sup> In order to investigate the interplay among these three MEG mechanisms, we are extending our current model to include matter–light interaction<sup>22,25</sup> and to treat more accurately the phonon-induced electron relaxation<sup>4,66</sup> and pure-dephasing<sup>64,65</sup> processes.

**Multiple Exciton Recombination.** The MER process is the inverse of MEG.<sup>24,35,44–48</sup> During MER, the two SEs forming a DE recombine, creating a high-energy SE. The current work reports two types of MER simulations. This subsection considers MER starting from a single DE state, in accord with the earlier theories.<sup>20,67,68</sup> Two subsections below we discuss MER that follows MEG, which agrees better with the experimental measurements.<sup>36,46–48</sup> DEs are optically inactive at the single-particle level of description. Therefore, they are produced in optical experiments by creating SEs that undergo MEG. Alternatively, DEs can be generated by two independent single-photon transitions. Requiring high light intensity, the latter process masks MEG, and hence, efforts are made to eliminate it in the MEG/MER studies. Regardless of the experimental procedure, it is virtually impossible to

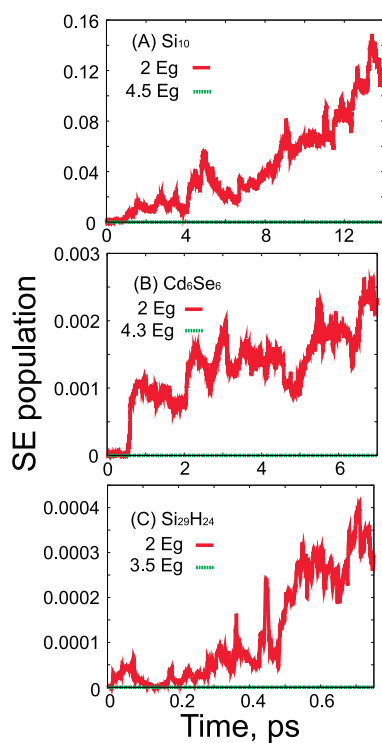


**Figure 5.** Growth of the total population of all SE states starting from a DE state of the energy indicated in the figure. The growth is due to MER. MER becomes efficient only at energies near  $2E_g$ . The MER dynamics is faster in  $\text{Si}_{10}$  than in  $\text{Cd}_6\text{Se}_6$ .  $\text{Si}_{29}\text{H}_{24}$  shows the slowest MER.

create just one DE state, due to a very high DE DOS (Figure 2). Therefore, initial conditions involving superpositions of DEs are more realistic than a single initial DE.

Figure 5 illustrates the MER dynamics starting from a DE state of the shown energy. The figure plots the total population of all SE states as a function of time and considers initial DE states that are both close to  $2E_g$  and higher in energy. Our simulation demonstrates that MER is possible only starting from low-energy DEs. Thus, higher-energy DEs need to lose some of their energy to phonons before they can annihilate and form SEs. Since our simulation takes into account both MEG and MER, the overall dynamics is determined by the relative values of the SE and DE DOS at a given energy. SEs can generate DEs at higher energies, while DEs can effectively annihilate to form SEs at lower energies. This is in harmony with the earlier reports,<sup>23,28</sup> which suggest that MER proceeds through lower-energy DEs. Phonon modes play a particularly important role in MER dynamics since MER is intimately coupled to electron–phonon relaxation. Not only must higher-energy DEs relax by coupling to phonons in order to achieve efficient MER, but also SEs formed during MERs lose their energy to phonons and, therefore, cannot recreate DEs due to energy conservation.

Extrapolation of the short time results shown in Figure 5 gives MER time on the order of tens to hundreds

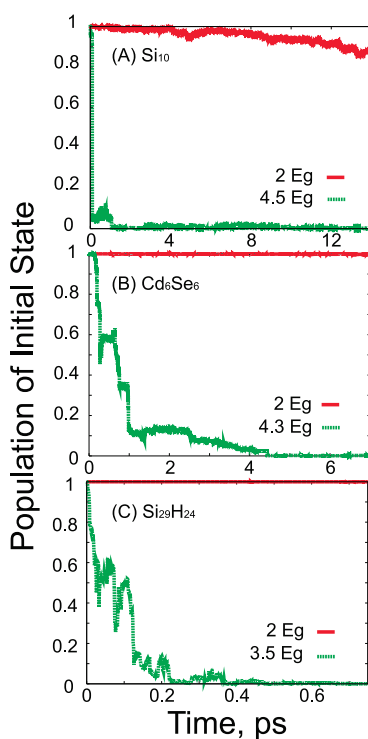


**Figure 6.** Population decay of the initially excited DE states. The decay is faster at higher energies. Note that at high energies the decay of the population of the initially excited DE states is not due to MER (Figure 5), but rather is a result of population transfer from the initial DE to other DEs.

of picoseconds, in agreement with the earlier calculations.<sup>20,67,68</sup> Among the three QDs considered here, the MER dynamics is slowest in the largest  $\text{Si}_{29}\text{H}_{24}$  cluster. This is in accordance with the experimental results.<sup>46–48,55</sup> Both the SE to DE DOS ratio and the electron–hole Coulomb interaction strength decrease with increasing cluster size, slowing down the MER process.

The evolution of the population of the initially excited DE states is shown in Figure 6. Just as with MEG (Figures 3 and 4), the evolution of the initial state population differs notably from the rate of the overall process. In the current case, as the energy increases, MER slows down (Figure 5), while the decay of the initial DE state population speeds up (Figure 6). At high energies, the initial DE transitions to other DEs rather than into SEs. In contrast, at low energies, the decrease of the population of the initial DE state (red line in Figure 6) is closely linked to the growth of the total population of all SEs (red line in Figure 5). This analysis supports the conclusion that lower-energy DEs constitute the main gateway to SEs via MER.

**Phonon Modes.** In contrast to many other models, the current simulation explicitly includes phonon dynamics and electron–phonon coupling. In particular, it allows for phonon-assisted Auger processes. The electron–phonon coupling is equivalent in the current simulation to the NA coupling (eq 4), which arises due to dependence of the electronic eigenstates on nuclear

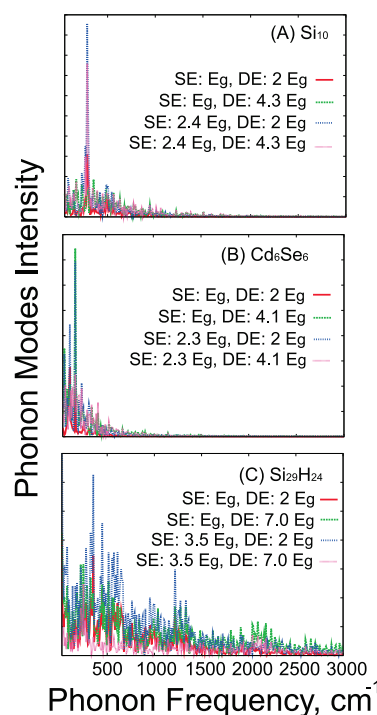


**Figure 7.** Phonon modes that couple the SE and DE state pairs indicated in the figure. The frequencies of the main peaks are higher in  $\text{Si}_{10}$  than in  $\text{Cd}_6\text{Se}_6$ , due to a smaller mass of the Si atom.  $\text{Si}_{29}\text{H}_{24}$  exhibits a broad phonon spectrum. The frequencies above  $1000 \text{ cm}^{-1}$  are due to Si–H motions.

coordinates. Fourier transforms of the fluctuations in the energy gaps between SE and DE states along the nuclear trajectory identify the frequencies of the phonons that couple to the Auger dynamics. The data are presented in Figure 7. The simulation shows that modes with frequencies above  $100 \text{ cm}^{-1}$  couple more strongly to the electrons and holes than the low-frequency modes. This is reasonable since the NA electron–phonon coupling (eq 4) is proportional to the nuclear velocity, and at a fixed temperature or energy, higher-frequency modes have larger velocities than lower-frequency modes. Moreover, by energy conservation, higher-energy phonons couple to a broader range of electronic states via the phonon-assisted Auger mechanism. The  $\text{Si}_{10}$  phonons are higher in frequency than the  $\text{Cd}_6\text{Se}_6$  phonons (Figure 7A,B), contributing to the faster MEG and MER dynamics in the  $\text{Si}_{10}$  QD (Figures 3 and 5, respectively).

The role of high-frequency modes is emphasized in the presence of ligands because most ligands are composed of atoms that are much lighter than the atoms forming the QD core. Hydrogens passivating the  $\text{Si}_{29}\text{H}_{24}$  QD surface introduce additional, high-frequency modes extending to  $2000 \text{ cm}^{-1}$  (Figure 7C). The stretching and bending motions involving hydrogens contribute to phonon-assisted Auger processes and are particularly important for MEG at energies below  $2E_g$  (Figure 3). The ligand contribution to the QD electronic states and electron–phonon coupling decrease with increasing QD size, resulting in a

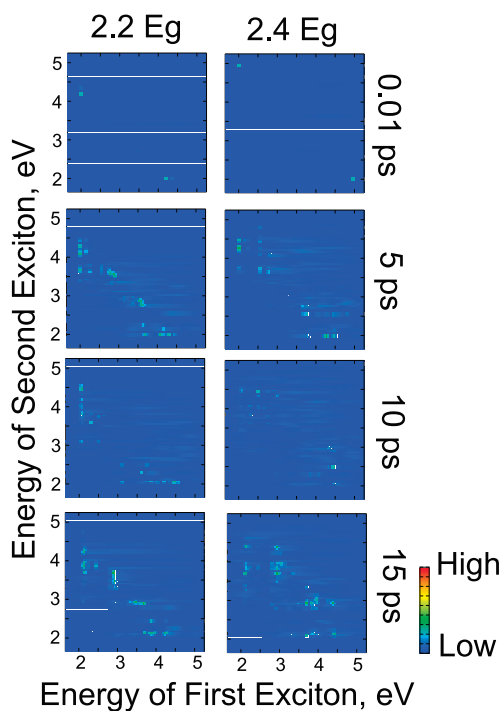


**Figure 8.** Evolution of the two excitons forming DE states in  $\text{Si}_{10}$ . The dynamics starts in a high-energy SE. By 0.01 ps, DEs are generated by creation of a second exciton at  $E_g$ . Creation of the second exciton is accompanied by decrease of the first exciton energy to the value displayed at the top. The subsequent evolution of the two excitons in the DE state occurs by diffusion along the constant energy line. The diffusion involves more states at higher energies.

reduced surface-to-volume ratio. The ligand contribution depends on the alignment of the ligand electronic energy levels with those of the QD core. Typically, the HOMO–LUMO gaps are larger in ligands than in the core. Therefore, ligands start contributing to the electronic and vibrational properties of semiconducting QDs at energies that are larger than the QD core band gap. By changing the chemistry of the ligands, one can fine-tune the phonon modes and energy ranges where ligands contribute to the Auger dynamics.

**Interplay between Multiple Exciton Generation and Recombination Dynamics.** Our simulation includes simultaneously a variety of processes, allowing us to study the interplay between MEG and MER and to provide additional details of the combined MEG/MER dynamics. In particular, we demonstrate that MER following MEG occurs faster than MER starting from a single DE state because a superposition of multiple DEs present after MEG can couple to larger number of SEs. This result is particularly important since it brings theory<sup>20,67,68</sup> in agreement with experiment.<sup>36,46–48</sup>

MEG converts one high-energy SE into two lower-energy SEs that form a DE. The evolution of DEs formed by this process is illustrated in Figures 8 and 9. The figures show a two-dimensional (2D) representation of the dynamics of the two SEs that form a DE, illustrating the diffusion of the excitons in the energy manifold. Figure 8 focuses on the smaller  $\text{Si}_{10}$  QD, while Figure 9

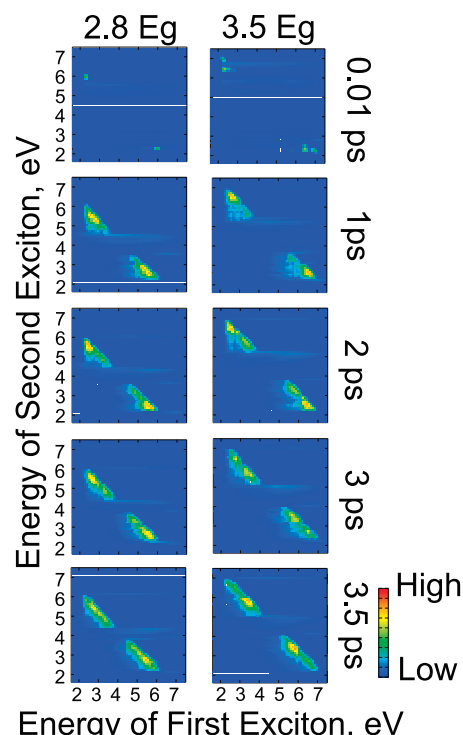


**Figure 9.** Same as Figure 8 but for  $\text{Si}_{29}\text{H}_{24}$ . Here, the DE DOS is high (Figure 2), and the population spreads rapidly over a larger number of DEs.

represents the larger  $\text{Si}_{29}\text{H}_{24}$  QD. Two different energies are considered in each case. The 2D maps are symmetric with respect to the diagonal because the first and second excitons are indistinguishable. At early times, the high-energy SE forms few DEs, as indicated by a small number of dots in the top panels of the figures. The DEs appear asymmetrically, rather than around the center of the 2D map. The second SE created during MEG has energy that is close to  $E_g$ . This result agrees well with the impact ionization mechanism and the experimental expectations.<sup>21,23,28,31–33,36</sup> With time, the initial DE diffuses along the constant energy line toward the center of the 2D map, where the two SEs forming DE have similar energies. Higher energies produce broader distributions of DEs since DE DOS rapidly grows with energy (Figure 2).

A number of differences can be observed in the DE diffusion of the smaller and larger Si QDs (Figures 8 and 9, respectively). Due to a relatively low DOS, the DE diffusion in  $\text{Si}_{10}$  is more random. Not all DEs are equally strongly coupled to each other, and there exist energy regions where SE DOS decreases rather than increases with energy (Figure 2A). The DE diffusion is smoother in the  $\text{Si}_{29}\text{H}_{24}$  QD. At the higher energy (right-hand side of Figure 9), the initial peak at (2.5 eV, 7 eV) disappears to form a new peak at (3.5 eV, 6 eV) on the 2D map. A similar phenomenon is seen in the higher-energy simulation of  $\text{Si}_{10}$ . The initial peak at (2 eV, 5 eV) spreads by 5 ps and refocuses at (2.5 eV, 4.5 eV) by 10 ps. Unlike  $\text{Si}_{10}$ , in which

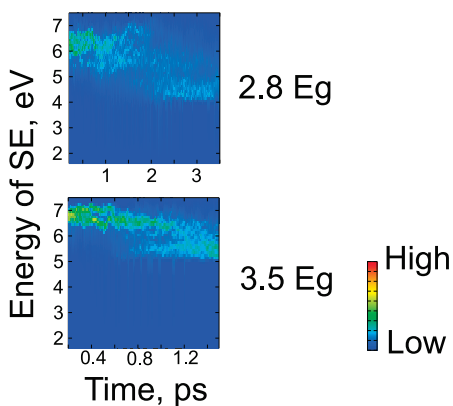


**Figure 10.** SE population dynamics accompanying DE dynamics shown in Figure 9. At early times, the initially excited SE diffuses into both other SE and DEs. The decrease of the SE population seen in the middle of each figure corresponds to MEG (Figure 3). The reappearance of the SE populations at the later time corresponds to MER, demonstrating that our method accounts simultaneously for both MEG and MER. The MER time scale observed here agree with the experiment; see the data for small QDs in Figure 3b of ref 48 and Figure 4 of ref 47. At the same time, it is much faster than the MER time scales seen in Figure 5, which correspond to the earlier theoretical calculations.<sup>20,67,68</sup> The difference resides in the fact that here MER occurs from DE states that are superpositions of a large number of individual DEs, while the results shown in Figure 5 and refs 20, 67, and 68 assume a single initial DE. Superpositions of DEs are able to access many more MER pathways, greatly increasing MER rate, and bringing theory and experiment into good agreement.

in  $\text{Si}_{29}\text{H}_{24}$  is created at the energy that is slightly higher than  $E_g = 2.1$  eV. This can be explained by the entropic effect. While it is more favorable energetically to create the second exciton close to  $E_g$ , the rapid increase of SE DOS with energy in the larger nanocrystal makes creation of SEs at a slightly higher energy more likely.

Figure 10 shows the SE population dynamics accompanying the DE generation displayed in Figure 9. Note that in contrast to Figures 8 and 9, in which both coordinates of the 2D map are SE energies, the SE population dynamics is displayed in Figure 10 as a 2D function of time and energy. At early times, the SE populations show diffusive dynamics, indicating that the initially excited SE evolves into other SEs. This is consistent with the discussion of Figure 4 above. At about 1 ps, the SE populations decrease due to MEG. This result agrees with the rise of the DE signal at 1 ps in Figure 9, as well as with the accelerating MEG in Figure 3C.

Most interestingly, the SE populations start to reappear in Figure 10 at a lower energy within a few picoseconds. The reappearance of the SE population is a result of MER. The sub-10 ps MER time agrees with the experiments.<sup>36,46–48</sup> The MER time depends on the QD size, and QDs whose diameters are smaller than 2 nm exhibit MER on a sub-10 ps time scale; see Figure 3b of ref 48 and Figure 4 of ref 47. Note that the sub-10 ps MER time scale obtained in the simulation described in Figure 10 is significantly shorter than the MER time scale deduced starting from a single DE (Figure 5).

Extrapolation of the data shown in Figure 5 gives MER time on the order of tens to hundreds of picoseconds, in agreement with the earlier rate estimates for small QDs<sup>20,67,68</sup> but in disagreement with the experimental data.<sup>36,46–48</sup> The difference stems from the fact that the MER process illustrated in Figure 10 involves a superposition of many DE states (see Figure 9). Compared to a single initial DE, a superposition of many DEs interacts with a significantly broader range of SEs via multiple coupling pathways. As a result, the MER rate increases substantially. Participation of a superposition of multiple initial states is particularly important for MER compared to MEG: the density of final states is much lower for MER than for MEG; compare the SE versus DE DOS in Figure 2, and therefore, it is very important to couple to as many final states as possible in order to achieve fast MER.

Incidentally, the diffusion of the excited state population in the QD electronic state manifold illustrated in Figures 8–10 is similar to the intramolecular vibrational energy redistribution (IVR), in which the population of an initially excited vibrational mode spreads to other modes.<sup>69,70</sup> In present, the electronic states are delocalized over the whole QD, while vibrational modes considered in IVR are often localized on different molecular fragments (e.g., C=O mode or O–H mode). IVR is particularly interesting when it leads to energy flow between spatially different parts of the molecule. A similar effect can be observed in QD systems provided that they are composed of distinct components, such as core and shell regions, ligands, substrate, etc.

## CONCLUDING REMARKS

In summary, we have performed a time-domain, atomistic, *ab initio* study of MEG and MER dynamics in semiconductor QDs of different size and material, with and without ligands. Particular focus is given to Si clusters because Si is the most popular solar cell material and MEG carries good potential for increasing photovoltaic efficiencies. By explicitly coupling ground, SE, and DE electronic states to phonon motion, we incorporate phonon-assisted Auger processes. At atomistic description lets us consider the effects of QD structure and surface passivation on the Auger dynamics. The time-domain representation describes various relaxation regimes, bypassing the limitations of rate models that implicitly assume exponential decay.

We show that MEG occurs on a picosecond time scale in the small QDs. The process speeds up considerably with energy since the ratio of the final DE to initial SE state densities grows with energy. Our simulation proves that MEG can occur at energies below the purely electronic energy threshold and that the electronic degrees of freedom can borrow energy from phonons. Such phonon-assisted MEG is best promoted by high-frequency phonons of surface ligands.

The time-domain picture provided by our simulation indicates that MEG in small QDs is Gaussian rather than exponential. The Gaussian amplitude decreases in larger clusters, and exponential relaxation becomes dominant. In combination with the fact that the electron–hole Coulomb interaction decreases in larger clusters, approaching the weak-coupling limit, this outcome of our work justifies the rate descriptions based on perturbation theory, such as Fermi's golden rule. MEG starts by transfer of population from the initially excited SE state to other SEs. The created superposition of many SEs is able to access a wider range of DEs, facilitating efficient and exponential MEG. The range of final DE states is further broadened by coupling to phonons, which lifts the strict energy conservation condition required for the purely electronic MEG.

High-frequency phonons participate most actively in MEG and MER. This fact can be rationalized by both the NA electron–phonon coupling and the energy conservation. The coupling is proportional to phonon velocity, and for a given temperature, the velocity is larger for higher-frequency modes. More energetic phonons require fewer quanta in order to exchange appreciable amounts of energy with the electronic subsystem and to broaden the allowed energy range of coupled SE and DE states. The role of high-frequency modes is emphasized in the presence of ligands because most ligands are composed of atoms that are much lighter than the atoms forming the QD core. The ligand contribution depends on the alignment of the electronic energy levels of the ligand and the QD core. Typically, ligand contributions start at energies that are some energy away from the valence and conduction band edges of the semiconductor material. One can tune the ligand contributions by chemical means.

Phonon-assisted MEG is most easily observed at excitation energies below the purely electronic threshold of  $2E_g$ , particularly in the presence of high-frequency ligand phonons. Phonon-assisted MEG and MER can also happen at energies above the electronic threshold. However, it is difficult to observe these effects explicitly since they operate in parallel with the purely electronic Auger processes. One can attempt to distinguish phonon-assisted dynamics experimentally by temperature dependence because it should depend on temperature much more than purely electronic processes. In such studies, temperature should be sufficiently high to excite active phonon modes, which can be problematic for high-frequency phonons of ligands. Additionally, one

would need to differentiate between electron–phonon relaxation and phonon-assisted Auger processes because both would exhibit temperature dependence. The relaxation is continuous across the whole energy range, with a possible bottleneck close to  $E_g$ . In contrast, phonon-assisted Auger dynamics should undergo substantial changes at the  $2E_g$  threshold and larger multiple integers of  $E_g$ . Further, phonon-induced pure-dephasing resulting in loss of coherence in superpositions of electronic states, for instance, between SEs and DEs, should be differentiated, as well. In particular, pure-dephasing is elastic and does not involve electron–phonon energy exchange.

Electron–phonon relaxation is particularly important for MER. MER is efficient only at energies close to  $2E_g$ , where the SE DOS is higher than the DE DOS. Therefore, high-energy DEs must relax by coupling to phonons prior to recombination. In addition, SEs formed during MER must lose some of their energy to phonons in order to avoid regenerating DEs.

MER starting from a single DE state is significantly slower than MER simulated in accord with the experiments, in which optically excited SEs undergo MEG and then MER. MER starting from a DE requires tens to hundreds of picoseconds, in agreement with the earlier rate theory estimates for small QDs but in contradiction with the experimental data. MER following MEG requires under 10 ps, in agreement with the experiments. The second scenario produces much faster MER because a superposition of many DEs created during MEG is able to couple efficiently to multiple SEs.

The QDs used in our calculations are smaller than those typically employed in the experiments. As the QD size grows, the DE to SE DOS ratio increases, speeding up MEG and slowing down MER. These effects are seen in our simulations. The electron–hole Coulomb interaction strength decreases with increasing QD diameter, slowing down the Auger dynamics. The surface and ligand contributions to the QD electronic structure and Auger dynamics decrease with increasing QD size, reflecting the reduced surface-to-volume ratio and suppressing those phonon-assisted Auger processes that are facilitated by the high-frequency ligand vibrations.

The reported *ab initio* time-domain modeling of Auger processes provides a detailed and comprehensive picture of the coupled electron–phonon dynamics in semiconductor QDs, enhances our understanding of the properties and behavior of nanoscale materials in general, and provides valuable insights for the development of efficient light-harvesting devices and other applications.

## SIMULATION METHODS

The state-of-the-art simulations performed in the current work combine time-domain density functional theory (TDDFT) with nonadiabatic molecular dynamics (NAMD).<sup>4,10,24,66,71</sup>

The electronic structure and adiabatic MD were computed with VASP<sup>72</sup> using converged plane-wave basis in a cubic simulation cell. Spurious interactions of periodic images were prevented by including at least 8 Å of vacuum between QD replicas. The PW91

density functional and projector-augmented wave pseudopotentials were used. The QD geometry was generated from the corresponding bulk structure. The larger Si QD was passivated by hydrogen atoms. The systems were fully optimized at zero temperature and brought to ambient temperature by repeated velocity rescaling. Microcanonical trajectories of 5 to 30 ps in length were produced in the ground electronic state using the Verlet algorithm with a 1 fs time step.

The Auger dynamics involving SE and DE states coupled to the atomic motions were simulated using TDDFT formulated in the adiabatic Kohn–Sham (KS) basis.<sup>4,66,71</sup> Note that the adiabatic representation of the Auger dynamics differs from the more traditional picture, in which noninteracting electrons and holes scatter due to Coulomb interaction. In the adiabatic representation, the Coulomb coupling between electrons and holes is included in the Hamiltonian. In particular, the electron–hole interaction is part of the exchange-correlation functional of DFT. All electronic effects are “diagonalized out”. As a result, adiabatic electronic states attain dependence on phonon coordinates, and transitions between different SE and DE states occur due to the nonadiabatic (NA) coupling.

The evolution of the single-electron KS orbitals  $\phi_p(\mathbf{r}, t)$  was determined using the standard TDKS equations

$$i\hbar \frac{\partial \phi_p(\mathbf{r}, t)}{\partial t} = H(\phi(\mathbf{r}, t))\phi_p(\mathbf{r}, t), p = 1, \dots, N_e \quad (1)$$

where  $N_e$  is the number of electrons. The equations are coupled because the Hamiltonian  $H$  depends on the density obtained by summing over all occupied KS orbitals. Expanding the time-dependent KS orbitals  $\phi_p(\mathbf{r}, t)$  in the adiabatic KS orbital basis  $\tilde{\phi}_k(\mathbf{r}; \mathbf{R})$

$$\phi_p(\mathbf{r}, t) = \sum_{k=1}^{N_e} c_{pk}(t) |\tilde{\phi}_k(\mathbf{r}; \mathbf{R})\rangle \quad (2)$$

transforms the TDKS (eq 1) into the equations for the expansion coefficients

$$i\hbar \frac{\partial c_{pk}(t)}{\partial t} = \sum_{m=1}^{N_e} c_{pm}(t) (\epsilon_m \delta_{km} - i\hbar \mathbf{d}_{km} \cdot \dot{\mathbf{R}}) \quad (3)$$

The adiabatic KS orbitals  $\tilde{\phi}_k(\mathbf{r}; \mathbf{R})$  were obtained with DFT for current atomic positions along the MD trajectory. The NA coupling describes the electron–phonon interaction

$$\mathbf{d}_{km} \cdot \dot{\mathbf{R}} = \langle \tilde{\phi}_k(\mathbf{r}; \mathbf{R}) | \nabla_{\mathbf{R}} | \tilde{\phi}_m(\mathbf{r}; \mathbf{R}) \rangle \cdot \dot{\mathbf{R}} = \langle \tilde{\phi}_k(\mathbf{r}; \mathbf{R}) | \frac{\partial}{\partial t} | \tilde{\phi}_m(\mathbf{r}; \mathbf{R}) \rangle \quad (4)$$

It arises from the dependence of the adiabatic KS orbitals on the phonon dynamics  $\mathbf{R}(t)$ .

Our simulation included the ground, SE, and DE states,  $|\Phi_g(\mathbf{r}; \mathbf{R})\rangle$ ,  $|\Phi_{SE}^{i,j}(\mathbf{r}; \mathbf{R})\rangle$ , and  $|\Phi_{DE}^{i,j,k,l}(\mathbf{r}; \mathbf{R})\rangle$ , respectively, and was formulated using second quantization with the ground state as a reference.<sup>24</sup> SEs and DEs are obtained as

$$|\Phi_{SE}^{i,j}\rangle = \hat{a}_i^\dagger \hat{a}_j |\Phi_g\rangle, |\Phi_{DE}^{i,j,k,l}\rangle = \hat{a}_i^\dagger \hat{a}_j \hat{a}_k^\dagger \hat{a}_l |\Phi_g\rangle \quad (5)$$

where the electron creation and annihilation operators,  $\hat{a}_i^\dagger$  and  $\hat{a}_i$ , generate and destroy an electron in the  $i$ th and  $j$ th adiabatic KS orbitals, respectively. The time-evolving wave function is then expressed by

$$|\Psi(t)\rangle = C_g(t) |\Phi_g\rangle + \sum_{i,j} C_{SE}^{i,j}(t) |\Phi_{SE}^{i,j}\rangle + \sum_{i,j,k,l} C_{DE}^{i,j,k,l}(t) |\Phi_{DE}^{i,j,k,l}\rangle \quad (6)$$

Similarly to eq 3, the expansion coefficients appearing in eq 6 evolve by the first-order differential equations

$$\begin{aligned} i\hbar \frac{\partial C_X(t)}{\partial t} &= C_X(t) E_X - i\hbar C_g(t) \mathbf{d}_{X,g} \cdot \dot{\mathbf{R}} \\ &- i\hbar \sum_{i',j'} C_{SE}^{i',j'}(t) \mathbf{d}_{X,SE,i',j'} \cdot \dot{\mathbf{R}} \\ &- i\hbar \sum_{i',j',k',l'} C_{DE}^{i',j',k',l'}(t) \mathbf{d}_{X,DE,i',j',k',l'} \cdot \dot{\mathbf{R}} \end{aligned} \quad (7)$$

where  $X$  and  $Y$  now correspond to either ground, SE, or DE state,  $E_X$  is the state energy, and the NA couplings are defined by

$$\mathbf{d}_{X,Y} \cdot \dot{\mathbf{R}} \equiv \langle \Phi_X | \nabla_{\mathbf{R}} | \Phi_Y \rangle \cdot \dot{\mathbf{R}} = \langle \Phi_X | \frac{\partial}{\partial t} | \Phi_Y \rangle \quad (8)$$

The atomistic simulation of the SE/DE generation and recombination dynamics was performed by directly solving eq 7 with time-dependent NA couplings and energies.<sup>24</sup> The ground, SE, and DE states form the two-particle electronic basis in our method, and each state can transit to another state due to the NA coupling. The energies appear in the diagonal parts of the Hamiltonian, while the NA couplings are embedded in the corresponding off-diagonal components. The simulations are extremely large scale. For instance, the 24 CB and 25 VB orbitals used in our calculations on the Si<sub>29</sub>H<sub>24</sub> QD give rise to 600 SE and 97 500 DE states. The total number of states is 98 101, and the Hamiltonian appearing in the TD Schrödinger equation (eq 7) contains  $98 101^2 = 9 623 806 201$  matrix elements. It is too large for direct numerical simulation; however, the Hamiltonian is sparse since the NA couplings connect KS basis states that differ only in a single electron or hole.<sup>71</sup> On the basis of this fact, we developed an efficient simulation code that can remove all zero components from the sparse matrix, and solve eq 7 using only the extracted nonzero parts of the Hamiltonian.<sup>24</sup>

The method described above includes electron–phonon interactions and properly treats the transfer of energy from phonons to electrons encountered in phonon-assisted Auger dynamics. Described classically, the phonons create an external field that enters the quantum mechanical equation-of-motion for the electrons and influences the electron dynamics. Proper treatment of the reverse process involving energy transfer from the quantum mechanical electrons to the classical phonons constitutes the so-called quantum backreaction problem<sup>73,74</sup> and requires a more advanced technique, such as surface hopping (SH).<sup>71</sup> SH was used in our earlier simulations in order to study electron–phonon cooling, during which several electronvolts of electronic energy were deposited into vibrational degrees of freedom.<sup>4,66</sup> Currently, we are working to implement SH with the Auger processes, in order to study the interplay of the Auger dynamics with cooling. Further anticipated advances of the method include explicit interaction with light, which is needed in order to allow for the direct MEG mechanism, and quantum corrections for the phonon motion, which should be important for the high-frequency ligand modes.

**Acknowledgment.** K.H.D. is partially supported by the Global COE Program Integrated Materials Science (#B-09). O.V.P. acknowledges financial support of DOE, Grant No. DE-FG02-05ER15755, dedicated to the QD studies, and NSF, Grant No. CHE-1050405, supporting methods development.

## REFERENCES AND NOTES

- Nozik, A. J. Spectroscopy and Hot Electron Relaxation Dynamics in Semiconductor Quantum Wells and Quantum Dots. *Annu. Rev. Phys. Chem.* **2001**, 52, 193–231.
- Shockley, W.; Queisser, H. J. Detailed Balance Limit of Efficiency of p-n Junction Solar Cells. *J. Appl. Phys.* **1961**, 32, 510–519.
- Cooney, R. R.; Sewall, S. L.; Anderson, K. E. H.; Dias, E. A.; Kambhampati, P. Breaking the Phonon Bottleneck for Holes in Semiconductor Quantum Dots. *Phys. Rev. Lett.* **2007**, 98, 177403-1–177403-4.
- Kilina, S. V.; Kilin, D. S.; Prezhdo, O. V. Breaking the Phonon Bottleneck in PbSe and CdSe Quantum Dots: Time-Domain Density Functional Theory of Charge Carrier Relaxation. *ACS Nano* **2009**, 3, 93–99.
- Knowles, K. E.; McArthur, E. A.; Weiss, E. A. A Multi-Timescale Map of Radiative and Nonradiative Decay Pathways for Excitons in CdSe Quantum Dots. *ACS Nano* **2011**, 5, 2026–2035.
- Lupo, M. G.; Della Sala, F.; Carbone, L.; Zavelani-Rossi, M.; Fiore, A.; Luer, L.; Polli, D.; Cingolani, R.; Manna, L.; Lanzani, G. Ultrafast Electron–Hole Dynamics in Core/Shell CdSe/CdS Dot/Rod Nanocrystals. *Nano Lett.* **2008**, 8, 4582–4587.

7. Schaller, R. D.; Pietryga, J. M.; Goupalov, S. V.; Petruska, M. A.; Ivanov, S. A.; Klimov, V. I. Breaking the Phonon Bottleneck in Semiconductor Nanocrystals via Multiphoton Emission Induced by Intrinsic Nonadiabatic Interactions. *Phys. Rev. Lett.* **2005**, *95*, 196401-1–196401-4.
8. Kambhampati, P. Unraveling the Structure and Dynamics of Excitons in Semiconductor Quantum Dots. *Acc. Chem. Res.* **2011**, *44*, 1–13.
9. Pandey, A.; Guyot-Sionnest, P. Slow Electron Cooling in Colloidal Quantum Dots. *Science* **2008**, *322*, 929–932.
10. Prezhdo, O. V. Photoinduced Dynamics in Semiconductor Quantum Dots: Insights from Time-Domain *Ab Initio* Studies. *Acc. Chem. Res.* **2009**, *42*, 2005–2016.
11. Acharya, K. P.; Khon, E.; O'Conner, T.; Nemitz, I.; Klinkova, A.; Khnayzer, R. S.; Anzenbacher, P.; Zamkov, M. Heteroepitaxial Growth of Colloidal Nanocrystals onto Substrate Films via Hot-Injection Routes. *ACS Nano* **2011**, *5*, 4953–4964.
12. Tisdale, W. A.; Williams, K. J.; Timp, B. A.; Norris, D. J.; Aydil, E. S.; Zhu, X. Y. Hot-Electron Transfer from Semiconductor Nanocrystals. *Science* **2010**, *328*, 1543–1547.
13. Jin, S.; Song, N.; Lian, T. Suppressed Blinking Dynamics of Single QDs on ITO. *ACS Nano* **2010**, *4*, 1545–1552.
14. McGuire, J. A.; Joo, J.; Pietryga, J. M.; Schaller, R. D.; Klimov, V. I. New Aspects of Carrier Multiplication in Semiconductor Nanocrystals. *Acc. Chem. Res.* **2008**, *41*, 1810–1819.
15. Nozik, A. J. Quantum Dot Solar Cells. *Physica E* **2002**, *14*, 115–120.
16. Nozik, A. J. Multiple Exciton Generation in Semiconductor Quantum Dots. *Chem. Phys. Lett.* **2008**, *457*, 3–11.
17. Semonin, O. E.; Luther, J. M.; Choi, S.; Chen, H.-Y.; Gao, J.; Nozik, A. J.; Beard, M. C. Peak External Photocurrent Quantum Efficiency Exceeding 100% via MEG in a Quantum Dot Solar Cell. *Science* **2011**, *334*, 1530–1533.
18. Beard, M. C.; Knutson, K. P.; Yu, P. R.; Luther, J. M.; Song, Q.; Metzger, W. K.; Ellingson, R. J.; Nozik, A. J. Multiple Exciton Generation in Colloidal Silicon Nanocrystals. *Nano Lett.* **2007**, *7*, 2506–2512.
19. Beard, M. C.; Midgett, A. G.; Law, M.; Semonin, O. E.; Ellingson, R. J.; Nozik, A. J. Variations in the Quantum Efficiency of Multiple Exciton Generation for a Series of Chemically Treated PbSe Nanocrystal Films. *Nano Lett.* **2009**, *9*, 836–845.
20. Califano, M. Photoinduced Surface Trapping and the Observed Carrier Multiplication Yields in Static CdSe Nanocrystal Samples. *ACS Nano* **2011**, *5*, 3614–3621.
21. Ellingson, R. J.; Beard, M. C.; Johnson, J. C.; Yu, P. R.; Micic, O. I.; Nozik, A. J.; Shabaev, A.; Efros, A. L. Highly Efficient Multiple Exciton Generation in Colloidal PbSe and PbS Quantum Dots. *Nano Lett.* **2005**, *5*, 865–871.
22. Fischer, S. A.; Isborn, C. M.; Prezhdo, O. V. Excited States and Optical Absorption of Small Semiconducting Clusters: Dopants, Defects and Charging. *Chem. Sci.* **2011**, *2*, 400–406.
23. Franceschetti, A.; An, J. M.; Zunger, A. Impact Ionization Can Explain Carrier Multiplication in PbSe Quantum Dots. *Nano Lett.* **2006**, *6*, 2191–2195.
24. Hyeon-Deuk, K.; Prezhdo, O. V. Time-Domain *Ab Initio* Study of Auger and Phonon-Assisted Auger Processes in a Semiconductor Quantum Dot. *Nano Lett.* **2011**, *11*, 1845–1850.
25. Isborn, C. M.; Kilina, S. V.; Li, X.; Prezhdo, O. V. Generation of Multiple Excitons in PbSe and CdSe Quantum Dots by Direct Photoexcitation: First-Principles Calculations on Small PbSe and CdSe Clusters. *J. Phys. Chem. C* **2008**, *112*, 18291–18294.
26. Ji, M.; Park, S.; Connor, S. T.; Mokari, T.; Cui, Y.; Gaffney, K. J. Efficient Multiple Exciton Generation Observed in Colloidal PbSe Quantum Dots with Temporally and Spectrally Resolved Intraband Excitation. *Nano Lett.* **2009**, *9*, 1217–1222.
27. Lin, Z.; Franceschetti, A.; Lusk, M. T. Size Dependence of the Multiple Exciton Generation Rate in CdSe Quantum Dots. *ACS Nano* **2011**, *5*, 2503–2511.
28. Luo, J. W.; Franceschetti, A.; Zunger, A. Carrier Multiplication in Semiconductor Nanocrystals: Theoretical Screening of Candidate Materials Based on Band-Structure Effects. *Nano Lett.* **2008**, *8*, 3174–3181.
29. Murphy, J. E.; Beard, M. C.; Norman, A. G.; Ahrenkiel, S. P.; Johnson, J. C.; Yu, P. R.; Micic, O. I.; Ellingson, R. J.; Nozik, A. J. PbTe Colloidal Nanocrystals: Synthesis, Characterization, and Multiple Exciton Generation. *J. Am. Chem. Soc.* **2006**, *128*, 3241–3247.
30. Piryatinski, A.; Velizhanin, K. A. An Exciton Scattering Model for Carrier Multiplication in Semiconductor Nanocrystals: Theory. *J. Chem. Phys.* **2010**, *133*, 084508-1–084508-19.
31. Rabani, E.; Baer, R. Distribution of Multiexciton Generation Rates in CdSe and InAs Nanocrystals. *Nano Lett.* **2008**, *8*, 4488–4492.
32. Rabani, E.; Baer, R. Theory of Multiexciton Generation in Semiconductor Nanocrystals. *Chem. Phys. Lett.* **2010**, *496*, 227–235.
33. Schaller, R. D.; Klimov, V. I. High Efficiency Carrier Multiplication in PbSe Nanocrystals: Implications for Solar Energy Conversion. *Phys. Rev. Lett.* **2004**, *92*, 186601-1–186601-4.
34. Schaller, R. D.; Agranovich, V. M.; Klimov, V. I. High-Efficiency Carrier Multiplication through Direct Photogeneration of Multi-Excitons via Virtual Single-Exciton States. *Nat. Phys.* **2005**, *1*, 189–194.
35. Califano, M. Direct and Inverse Auger Processes in InAs Nanocrystals: Can the Decay Signature of a Trion Be Mistaken for Carrier Multiplication? *ACS Nano* **2009**, *3*, 2706–2714.
36. Schaller, R. D.; Pietryga, J. M.; Klimov, V. I. Carrier Multiplication in InAs Nanocrystal Quantum Dots with an Onset Defined by the Energy Conservation Limit. *Nano Lett.* **2007**, *7*, 3469–3476.
37. Baer, R.; Rabani, E. Can Impact Excitation Explain Efficient Carrier Multiplication in Carbon Nanotube Photodiodes? *Nano Lett.* **2010**, *10*, 3277–3282.
38. Gabor, N. M.; Zhong, Z.; Bosnick, K.; Park, J.; McEuen, P. L. Extremely Efficient Multiple Electron–Hole Pair Generation in Carbon Nanotube Photodiodes. *Science* **2009**, *325*, 1367–1371.
39. Johnson, J. C.; Nozik, A. J.; Michl, J. High Triplet Yield from Singlet Fission in a Thin Film of 1,3-Diphenylisobenzofuran. *J. Am. Chem. Soc.* **2010**, *132*, 16302–16303.
40. Ueda, A.; Matsuda, K.; Tayagaki, T.; Kanemitsua, Y. Carrier Multiplication in Carbon Nanotubes Studied by Femtosecond Pump-Probe Spectroscopy. *Appl. Phys. Lett.* **2008**, *92*, 233105-1–233105-3.
41. Wang, S.; Khafizov, M.; Tu, X.; Zheng, M.; Krauss, T. D. Multiple Exciton Generation in Single-Walled Carbon Nanotubes. *Nano Lett.* **2010**, *10*, 2381–2386.
42. Beard, M. C.; Midgett, A. G.; Hanna, M. C.; Luther, J. M.; Hughes, B. K.; Nozik, A. J. Comparing Multiple Exciton Generation in Quantum Dots To Impact Ionization in Bulk Semiconductors: Implications for Enhancement of Solar Energy Conversion. *Nano Lett.* **2010**, *10*, 3019–3027.
43. Huang, L. B.; Krauss, T. D. Quantized Bimolecular Auger Recombination of Excitons in Single-Walled Carbon Nanotubes. *Phys. Rev. Lett.* **2006**, *96*, 057407-1–057407-4.
44. Ivanov, S. A.; Achermann, M. Spectral and Dynamic Properties of Excitons and Biexcitons in Type-II Semiconductor Nanocrystals. *ACS Nano* **2010**, *4*, 5994–6000.
45. Jha, P. P.; Guyot-Sionnest, P. Trion Decay in Colloidal Quantum Dots. *ACS Nano* **2009**, *3*, 1011–1015.
46. Kobayashi, Y.; Pan, L.; Tamai, N. Effects of Size and Capping Reagents on Biexciton Auger Recombination Dynamics of CdTe Quantum Dots. *J. Phys. Chem. C* **2009**, *113*, 11783–11789.
47. Kobayashi, Y.; Nishimura, T.; Yamaguchi, H.; Tamai, N. Effect of Surface Defects on Auger Recombination in Colloidal CdS Quantum Dots. *J. Phys. Chem. Lett.* **2011**, *2*, 1051–1055.
48. Robel, I.; Gresback, R.; Kortshagen, U.; Schaller, R. D.; Klimov, V. I. Universal Size-Dependent Trend in Auger Recombination in Direct-Gap and Indirect-Gap Semiconductor Nanocrystals. *Phys. Rev. Lett.* **2009**, *102*, 177404-1–177404-4.

49. Ben-Lulu, M.; Mocatta, D.; Bonn, M.; Banin, U.; Ruhman, S. On the Absence of Detectable Carrier Multiplication in a Transient Absorption Study of InAs/CdSe/ZnSe Core/Shell1/Shell2 Quantum Dots. *Nano Lett.* **2008**, *8*, 1207–1211.
50. McGuire, J. A.; Sykora, M.; Joo, J.; Pietryga, J. M.; Klimov, V. I. Apparent versus True Carrier Multiplication Yields in Semiconductor Nanocrystals. *Nano Lett.* **2010**, *10*, 2049–2057.
51. Nair, G.; Bawendi, M. G. Carrier Multiplication Yields of CdSe and CdTe Nanocrystals by Transient Photoluminescence Spectroscopy. *Phys. Rev. B* **2007**, *76*, 08134–1–08134–4.
52. Nair, G.; Geyer, S. M.; Chang, L.-Y.; Bawendi, M. G. Carrier Multiplication Yields in PbS and PbSe Nanocrystals Measured by Transient Photoluminescence. *Phys. Rev. B* **2008**, *78*, 125325-1–125325-10.
53. Pijpers, J. J. H.; Ulbricht, R.; Tielrooij, K. J.; Osherov, A.; Golan, Y.; Delerue, C.; Allan, G.; Bonn, M. Assessment of Carrier-Multiplication Efficiency in Bulk PbSe and PbS. *Nat. Phys.* **2009**, *5*, 811–814.
54. Trinh, M. T.; Houtepen, A. J.; Schins, J. M.; Hanrath, T.; Piris, J.; Knulst, W.; Goossens, A. P. L. M.; Siebbeles, L. D. A. In Spite of Recent Doubts Carrier Multiplication Does Occur in PbSe Nanocrystals. *Nano Lett.* **2008**, *8*, 1713–1718.
55. Tyagi, P.; Kambhampati, P. False Multiple Exciton Recombination and Multiple Exciton Generation Signals in Semiconductor Quantum Dots Arise from Surface Charge Trapping. *J. Chem. Phys.* **2011**, *134*, 094706-1–094706-10.
56. Evans, C. M.; Guo, L.; Peterson, J. J.; Maccagnano-Zacher, S.; Krauss, T. D. Ultrabright PbSe Magic-Sized Clusters. *Nano Lett.* **2008**, *8*, 2896–2899.
57. Teo, B. K.; Sloane, N. J. A. Magic Numbers in Polygonal and Polyhedral Clusters. *Inorg. Chem.* **1985**, *24*, 4545–4558.
58. Peterson, J. J.; Krauss, T. D. Fluorescence Spectroscopy of Single Lead Sulfide Quantum Dots. *Nano Lett.* **2006**, *6*, 510–514.
59. Moreels, I.; Lambert, K.; Smeets, D.; De Muynck, D.; Nollet, T.; Martins, J. C.; Vanhaecke, F.; Vantomme, A.; Delerue, C.; Allan, G.; et al. Size-Dependent Optical Properties of Colloidal PbS Quantum Dots. *ACS Nano* **2009**, *3*, 3023–3030.
60. Nirmal, M.; Dabbousi, B. O.; Bawendi, M. G.; Macklin, J. J.; Trautman, J. K.; Harris, T. D.; Brus, L. E. Fluorescence Intermittency in Single Cadmium Selenide Nanocrystals. *Nature* **1996**, *383*, 802–804.
61. Sykora, M.; Mangolini, L.; Schaller, R. D.; Kortshagen, U.; Jurbergs, D.; Klimov, V. I. Size-Dependent Intrinsic Radiative Decay Rates of Silicon Nanocrystals at Large Confinement Energies. *Phys. Rev. Lett.* **2008**, *100*, 067401-1–067401-4.
62. Nakazato, H.; Namiki, M.; Pascazio, S.; Rauch, H. On the Quantum Zeno Effect. *Phys. Lett. A* **1995**, *199*, 27–32.
63. Prezhdo, O. V.; Rossky, P. J. Quantum Decoherence and Short Time Solvent Response. *Phys. Rev. Lett.* **1998**, *81*, 5294.
64. Kamisaka, H.; Kilina, S. V.; Yamashita, K.; Prezhdo, O. V. Ultrafast vibrationally-induced Dephasing of Electronic Excitations in PbSe Quantum Dot. *Nano Lett.* **2006**, *6*, 2295–2300.
65. Madrid, A. B.; Hyeon-Deuk, K.; Prezhdo, O. V. Phonon-Induced Dephasing of Excitons in Semiconductor Quantum Dots: Multiple Exciton Generation, Fission, and Luminescence. *ACS Nano* **2009**, *3*, 2487–2494.
66. Hyeon-Deuk, K.; Prezhdo, O. V. Symmetric Band Structures and Asymmetric Ultrafast Electron and Hole Relaxations in Silicon and Germanium Quantum Dots: Time-Domain *Ab Initio* Simulation. *Dalton Trans.* **2009**, *45*, 10069–10077.
67. Califano, M.; Zunger, A.; Franceschetti, A. Efficient Inverse Auger Recombination at Threshold in CdSe Nanocrystals. *Nano Lett.* **2004**, *4*, 525–531.
68. Wang, L.-W.; Califano, M.; Zunger, A.; Franceschetti, A. Pseudopotential Theory of Auger Processes in CdSe Quantum Dots. *Phys. Rev. Lett.* **2003**, *91*, 056404-1–056404-4.
69. Sun, L. P.; Song, K. Y.; Hase, W. L. A S(N)2 Reaction that Avoids Its Deep Potential Energy Minimum. *Science* **2002**, *296*, 875–878.
70. Nesbitt, D. J.; Field, R. W. Vibrational Energy Flow in Highly Excited Molecules: Role of Intramolecular Vibrational Redistribution. *J. Phys. Chem.* **1996**, *100*, 12735–12756.
71. Craig, C. F.; Duncan, W. R.; Prezhdo, O. V. Trajectory Surface Hopping in the Time-Dependent Kohn-Sham Approach for Electron-Nuclear Dynamics. *Phys. Rev. Lett.* **2005**, *95*, 163001-1–163001-4.
72. Kresse, G.; Furthmuller, J. Efficiency of *Ab Initio* Total Energy Calculations for Metals and Semiconductors Using a Plane-Wave Basis Set. *Comput. Mater. Sci.* **1996**, *6*, 15–50.
73. Prezhdo, O. V. A Quantum-Classical Bracket that Satisfies the Jacobi Identity. *J. Chem. Phys.* **2006**, *124*, 201104-1–201104-4.
74. Prezhdo, O. V.; Brooksby, C. Quantum Backreaction through the Bohmian Particle. *Phys. Rev. Lett.* **2001**, *86*, 3215–3219.